Journal of Applied Life Sciences International

25(1): 19-36, 2022; Article no.JALSI.85282
ISSN: 2394-1103

Geochronology of Recent Sediments from the Upper Bonny Estuary (Niger Delta) Using Naturally Occurring Radionuclides

Omokheyeke Omorotionmwan [a] and Victor Ighariemu [b*]

[a] Centre for Marine Pollution Monitoring and Seafood Safety, University of Port Harcourt, Nigeria.
[b] Environmental Toxicology Unit, Department of Biochemistry, Faculty of Science, University of Port Harcourt, P.M.B 5323, Choba Rivers State, Nigeria.

Authors' contributions

This work was carried out in collaboration between both authors. Both authors read and approved the final manuscript.

Article Information

DOI: 10.9734/JALSI/2022/v25i130280

Open Peer Review History:
This journal follows the Advanced Open Peer Review policy. Identity of the Reviewers, Editor(s) and additional Reviewers, peer review comments, different versions of the manuscript, comments of the editors, etc are available here: https://www.sdiarticle5.com/review-history/85282

Original Research Article

Received 27 January 2022
Accepted 01 April 2022
Published 12 April 2022

ABSTRACT

The research evaluated temporal trends of naturally occurring radionuclides and their vertical distributions in sediment cores collected from three sites of diverse sedimentation regimes in Bonny Estuary, and developed and implemented sediment dating with unsupported lead-210. Radium (Ra) isotopes exhibited a very similar distribution throughout all sampled cores in each month, with ^{228}Ra, while ^{226}Ra displayed some variability with generally lower specific activities in dry months than in wet months. The values found in the study were all less than unity ranging from 0.3 to 0.8, which suggested sediment accretion and that the study area corresponded to zones with different sedimentation regimes. Temporal distribution of total ^{210}Pb in the sampled cores determined via its daughter ^{210}Po by alpha spectrometry assumed that the secular equilibrium between both radionuclides was achieved. However, the activities in Station 3 were found to be lower than those in Station 1, with Station 2 having the lowest activity registered in the samples collected in December month. The specific activities of ^{228}Ac (^{228}Ra), ^{212}Pb (^{228}Th) and ^{40}K against depth in the sampled cores were observed to be almost equal to one another at each stratigraphic interval. The average sedimentation rate throughout the core obtained from Constant Rate of Supply model ($0.068 \pm 0.015 g.cm^{-2}.y^{-1}$) was nearly the same as that obtained from the Constant Initial Concentration model (0.065 ± 0.004). However, the estimated ages were quite variable with depths

**Corresponding author: E-mail: victorighariemu@gmail.com;*

of various stratigraphic layers. The age of the sediment core was dated approximately 80 years, which was qualitatively validated using ^{137}CS whose activity was definitely undetected in the basal part of the core. The sedimentation rates calculated suggested low sedimentation characterized by low energy environment dominated by weak tidal currents.

Keywords: Sedimentation; radionuclides; upper bonny estuary; Niger Delta.

1. INTRODUCTION

Natural radioactive materials (NORM) can be found practically anywhere. Many geologic materials include NORM, which is why it is encountered during geological activities. NORM found in hydrocarbon exploration and production come from underground deposits containing radioactive elements like uranium and thorium, as well as their daughter products ^{226}Ra and ^{228}Ra. [1,2]. Various operational procedures used in the exploration and extraction processes contribute to or trigger NORM occurrence. These include mapping methods using remote sensing, explosives used in seismic exploration, drilling equipment, and downhole geophysical logging systems. Radioactive marker bullets are sometimes used to assist with relative depth estimations. After the casing has been placed, the gamma ray log is utilized to find the rounds. For the aim of correlation, radioactive tracers are also employed to evaluate the effectiveness of well cementing and subsurface water and crude oil flow direction [3]. During secondary recovery operations, varying levels of radioisotopes may be administered to aid fluid flow.

Lead-210 is a ^{238}U decay radioisotope. Uranium-238 decays to ^{226}Ra, which has a half-life of 1600 years, after a half-life of 4.5109 years. Radon gas (^{222}Rn, t1/2=3.8 days) decays from radium-226 in rocks, soil, and saltwater, with part of it escaping into the atmosphere. Radon gas decays to particulate ^{210}Pb, which has a half-life of 22.3 years, after passing through a sequence of short-lived daughters. Rainfall (washout) or dry fallout can transport ^{210}Pb to the soil. Direct fallout is the most common way for ^{210}Pb to enter water bodies, however a small amount of unsupported ^{210}Pb may also reach lakes via watershed transfer.

In paleoenvironmental research that require an age-depth relationship for sediments deposited in the last 100-150 years, lead-210 dating has become a standard approach [4]. Classic papers, for example, address the formation and dispersion of ^{210}Pb in the environment, and Goldberg [5] advocated using ^{210}Pb as a chronological tool in earth science forty years ago. Since then, the stratigraphic distribution of ^{210}Pb activity in recent sediments has been estimated using both alpha and gamma counting approaches [6,7,8]. Several dating models became popular over the same time period [9]. Thousands of investigations have used the method to build recent sediment chronologies over the last four decades or so [10].

The Bonny Estuary (Fig.1), which is the study site, has been the focal point for a wide variety of human activities; including a major sea port, industrial, urban and recreational facilities. It is an important zone of great diversities and sediment transfer, which often form sinks for sediment moving downstream, alongshore or landwards. The research is aimed at determining levels of radionuclides in sediment samples from within the Bonny Estuary, evaluate the temporal trends of naturally occurring radionuclides and their vertical distributions in sediment cores collected from sites of diverse sedimentation regimes in the area, develop and implement sediment dating with the unsupported lead-210, assess the degree of catchment disturbance by comparing recent sedimentation rates with pre-European sedimentation rates.

1.1 Geology and Physiography of the Niger Delta Coastline

An excellent review of the general geology of the Niger Delta with reference to three aspects of the stratigraphy, sedimentation and structural geology from cretaceous to present carried out by Chima [12]. The formation of the proto Niger Delta started in the Campanian period while the formation of the modern delta was in the Eocene period, about 40 to 63 million years ago (Fig.2). The basin is located in the Gulf of Guinea between longitudes 50E and 80E, and latitudes 40N and 60N, and includes nearly half of the Nigerian coastline. It is Africa's and the world's largest wetland, with flat low-lying swampy terrain crisscrossed by meandering and anastomosing streams, rivers, and creeks, and three major stratigraphic units: the Benin Formation (primarily sandstones), the Agbada Formation (sandstones and shales), and the Akata Formation (shales) [13].

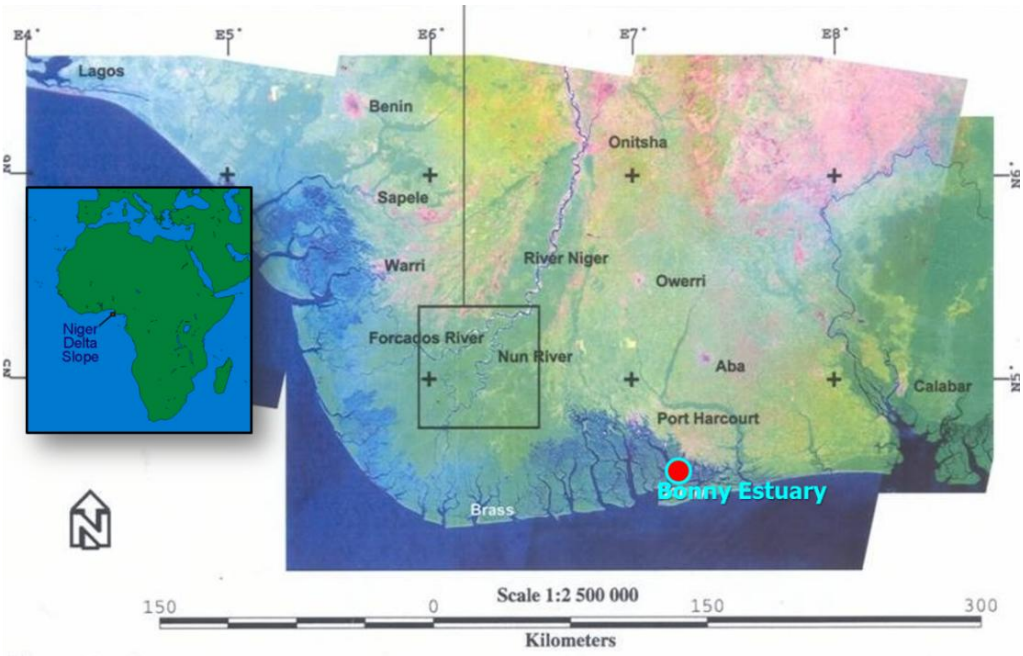

Fig. 1. Satellite Imagery of the Niger Delta showing the Bonny Estuary [11]

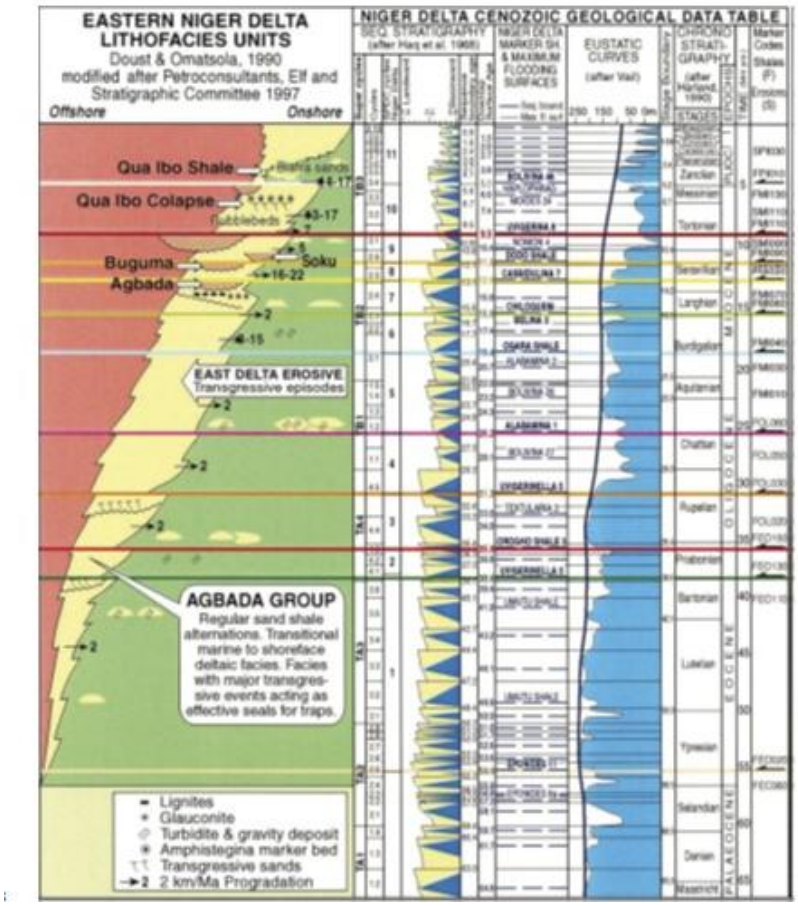

Fig. 2. Stratigraphic Column of the Eastern Niger Delta showing Lithofacies Units and Cenozoic Geological Data [14]

The coastline of the Niger Delta extends from the mouth of the Benin River in the west to the mouth of the Imo River in the east. It has twenty one (21) major channels from the Benin River to the Imo River namely Benin, Escravos, Forcados, Ramos, Dodo, Pennington, Digatoru, Bentagoru, Koluama, Fish Town, Sangana, Nun Brass, St. Nicholas, Santa Barbra, St. Bartholomew, Sombriero, New Calabar, Bonny, Andoni, and Imo Rivers. All of these open into the Atlantic Ocean [15] (Fig.1).

The Bonny River is one of the Niger Delta's numerous low-land coastal rivers. It is located in River State, Nigeria, between latitudes 40 25'N and 40 50'N, and longitudes 7000'E and 70 15'E. It's a short river, like most others, with a length of about 180 kilometers from mouth to mouth. It is bounded on the east by the Andoni basin's tidal split, on the northeast and north by the coastal plain sands of the river Sombreiro drainage, and on the west by the New Calabar River system's tidal waters. The river has a low relief of less than 50 kilometers above sea level [16], and it flows through a 730.24-hectare tidal marsh region [17].

The Bonny Estuary's river system includes a major river channel as well as numerous streams and creek-lets. It has the biggest tidal volume of all river systems in the Niger Delta (maximum width of 2km and maximum depth of around 15m near the mouth) and is mostly controlled by tidal movements [15]. This is due to the basin's low heights, simple tidal water entry, lack of fresh water discharge, and the basin's structure, which causes the tidal range to grow inland [15,18]. During the wet season, there is seasonality in the salinity of brackish water, particularly towards the limit of salt water intrusion; fresh water flow increases as rain fall increases. This shifts the boundary of salt water intrusion further out to sea, lowering salinity in brackish zones.

The delta is defined by sandy shorelines backed by large mangrove swamps and Barrier Island, which are separated by tidal canals. Semi-diurnal tidal regimes characterize the region, with a tidal amplitude of roughly 1.2m and ebb flow rates exceeding flood flow rates [15]. The tidal mudflat is a distinct feature of the area.

The Niger-Benue river system's delta structure is the most important drainage feature, draining around 60% of Nigeria and 34% of West Africa [13]. The Niger River, which drains much of West Africa, discharges its waters, sediments, and other burdens into the Niger Delta and, by extension, the Atlantic Ocean.

The delta's hydrology is controlled by three types of flow: unidirectional flow in the upper Niger Delta, bidirectional tidal flow in the coastal area and estuaries, and mixed flow in the transitional zone [19]. A typical hydrograph for the upper Niger Delta depicts a five-month dry season (December-April), followed by a gradual rise in water level, peaking around September/October. Because of their low elevation and structural links to the main drainage channel, the interior back marshes are regularly flooded before the peak floods. Because of the low gradient and permeability of the subsoil, the water that has accumulated in the back marshes rarely has a means to discharge or drain by gravity. Soon after reaching high water stage, the water level begins to drop dramatically, reaching its dry season level in less than 45 days. The exact discharge is determined on weather conditions.

The delta's coastline area is dominated by a daily rise and fall in water level, with a range of 1.8m to 2.75m in the west and east during spring tide, respectively. The Niger Delta receives between 2000 and 3000 millimeters of rain every year, with the majority of it falling between March and November. As one gets inland, rainfall falls dramatically. Between December and February, the dry season lasts fewer than three months. There are 2-3 days per month with rainfall of exceeding 1mm on average during these three months (Port Harcourt Metrological Service).

1.2 Measurement of Radionuclides in Sediments

The activity of unsupported ^{210}Pb can be assessed using one of two methods: alpha or gamma counts. Total ^{210}Pb activity must be determined in each stratigraphic sample down to a depth where there is no measurable unsupported ^{210}Pb. To get an estimate of unsupported ^{210}Pb activity, subtract supported ^{210}Pb activity from overall activity using an acceptable method. When it comes to assessing total and supported ^{210}Pb activity, the alpha and gamma counting approaches differ. The granddaughter radionuclide, ^{210}Po, can be used to determine total ^{210}Pb activity [6]. There are various advantages to using this strategy. Alpha detectors' great sensitivity makes them ideal for counting samples with little activity.

As a result, even in sediments with low bulk density, little amounts of material can be

employed, allowing for high-resolution (i.e. at small depth interval) counting. Additionally, alpha detectors are simple and inexpensive [4]. The alpha counting process, however, has a number of flaws. First, acid must be used to degrade the samples, and then the acid-extracted ^{210}Po must be plated on metal (Ag or Cu) disks. Second, throughout the chemical process, samples are destroyed. Third, in order to assess the efficiency of radioisotope plating on metal planchets, the wet chemical method necessitates the employment of a yield tracer (^{208}Po). Fourth, uppermost sediments should be kept for about two years before counting to ensure that ^{210}Pb and observed ^{210}Po are in balance.

1.3 Application of Radionuclides in Sediment Tracing

Environmental radionuclides are radionuclides that are found in the environment at low, quantifiable levels and are extensively distributed, including in sediments. They are, for the most part, of natural origin. Most work on environmental radionuclides for sediment tracing has concentrated on a specific set of radionuclides, specifically fallout radionuclides, or radionuclides that reach the land surface as fallout from the atmosphere. In general, the fallout input can be assumed to be spatially homogeneous, at least across a small area. Because the radionuclides used are promptly and strongly absorbed by the sediments as fallouts when they reach the catchment surface, they accumulate at or near the surface and can be used to track sediment mobilization and deposition. The use of unsupported or excess lead-210 (^{210}Pb) and ^{137}Cs as sediment tracers has mostly focused on these radionuclides. Lead-210 varies from ^{137}Cs in two key ways. First, ^{210}Pb is a naturally occurring radioactive element, and second, their fallout input can be assumed to remain virtually constant through time [20]. Lead-210 is frequently used as a chronological tool for sediments, while ^{137}Cs is used as a chronological marker, in combination with alpha and gamma counting techniques to estimate the stratigraphic distribution of the activity of a radionuclide of interest.

Regardless of how ^{210}Pb in sediments is detected or which dating model is used, precise estimation of unsupported (i.e. excess or atmospherically produced) ^{210}Pb activity at contiguous depths throughout the upper portion of a sediment core is required for the approach to work. The dating technique is made more difficult by the presence of supported ^{210}Pb in sediments. Supported ^{210}Pb, which is created by a decay-series precursor inside or linked to the sediment matrix, must be separated from atmospherically derived (unsupported or excess) ^{210}Pb. The ^{210}Pb activity is thought to be supported by in situ ^{226}Ra, with which it is thought to be in secular equilibrium. Local soil and bedrock particles, which are brought to the lake via colluviation, alleviation, or aeolian transport, are often the source of ^{226}Ra in the sediments.

1.4 Biological Influences on Sediment Homogeneity

Sediment systems sustain a diverse range of species, and their activities have a significant impact on overall sediment homogeneity. Almost every organism that lives in sediment interacts with its surroundings, modifying the sediment's features. The effects of such acts on sediment homogeneity vary widely, and study into specific species' influences is considerable. Widdows and Brinsley [21] classified macro fauna species as either sediment stabilisers or destabilisers (bio-stabilisers and bio-destabilisers). Bio-depositors, species that increase suspended particle deposition rates, may be included in stabilisers [22]. Bioturbation can also disrupt the sediment, making it less consolidated and rougher on the surface, lowering the critical erosion threshold [23, 24]. The ways in which animals interact with the sediment vary a lot, but they usually fall into one of many groups.

1.5 Sediment Yield and Transport

Sediment yield is caused by sediment systems in watersheds, as well as sediment transit via rivers. The amount of sediment traveling through a specific channel and site, which can be impacted by a variety of geomorphic features and processes, is referred to as sediment yield. It's possible that it'll be much less than the amount eroded in the basin. Sediment yield is calculated by dividing the total sediment volume delivered to a given site in the basin by the effective drainage area above that place for a given time period. Yield is usually expressed in cubic meters per square kilometer per year [25].

Sediment transport, on the other hand, is the movement of solid particles (sediment) caused by a combination of gravity acting on the sediment and/or the fluid in which the sediment is entrapped. Currents and tides transfer sediment in rivers, oceans, and lakes. The most common

application of sediment transport knowledge is to predict whether or not erosion or deposition will occur, as well as the magnitude of the erosion or deposition, and the time and distance over which it will occur [26]. Sediments carried to the Niger Delta basin in Nigeria originate from seven of the country's eight hydrological provinces: Niger North, Niger Central, Upper Benue, Lower Benue, Niger South, Western Littoral, Eastern Littoral, and Lake Chad. The catchment area of these seven provinces is 1413986 km" with a reservoir capacity of 29578.7 million m^3. Within the seven hydrological zones that directly affect the Niger Delta, there are a total of 135 small, medium, and major dams and reservoirs.

The sediment load of coast-bound flows is reduced as a result of the combined effect of reservoir sediment impoundment and increased in-channel sedimentation. Given that historical records of discharge distribution to the east and west deltas show a 55 percent preference for the west delta, sediment delivery to the western delta's coast is expected to be significantly higher. This lopsided distribution was maintained over the year 1983-1984, which coincided with a catastrophic drought in the Sahel and Sudan, when flow quantities were at their lowest in 40 years. Despite being much greater, the sediment transported to the western delta has not been enough to keep the area accreting. A comparison of satellite images of the coastal area from 1963 to 1988 reveals this, particularly in two critical river estuaries, the Forcados and Ramos Rivers, which together control 30% of the Niger River discharge. The huge sediment impoundment of dams, particularly Kainji, which was completed in 1968, is clear proof of the considerable shoreline recessions documented in this study.

Recent research by Ibe [27] has showed a net retreat of the shoreline in the eastern Niger Delta, with only minor accretion in the western Niger Delta. The eastern coastline's net erosion is explained by its non-direct connection to the Niger-Benue River system, which transports the majority of the sediments. Furthermore, in compared to their western counterparts, the Drainage Rivers in the eastern delta have a limited extent and catchment size. Because of the related greater coastal hydraulic forces, the erosion stress already experienced at the shore will become much worse with the expected rise in mean sea level. These coastal development patterns contrast with an earlier report, which reflected the pre-Kainji dam situation and showed a high level of erosion stress and a disruption in the existing ecological balance. Strong erosion stress indicated that not enough sediment was reaching some parts of the shore to maintain the ecological balance between erosive and constructive hydrological processes. With the constant entrapment of sediments, the dams have gradually silted up, reducing their ability to hold water. As a result, the dams can no longer act as flow barriers. Unless dam reservoirs are dredged to boost their holding capacity, flooding in downstream places is projected to return to pre-dam levels. Between 1968 and 1985, water levels plummeted as a result of heavy dam construction, but they're starting to rise again. Flooding was very bad in 1988 and 1994, causing residents to seek higher ground and destroying crops and homes. In comparison to the pre-dam years, however, the new flood water contains little or no silt.

1.6 Sediment Dating Models

Two ^{210}Pb dating models are now widely used. The constant initial concentration (CIC) model, which assumes a significant reservoir of unsupported ^{210}Pb in lake water. Regardless of the bulk sediment accumulation rate, the water column includes plentiful ^{210}Pb, according to this model. The rate of radioisotope scavenging in sediment is proportional to the rate of sediment deposition, which occurs in such a way that surface sediments always have the same beginning activity - hence the name of the model. The constant rate of supply (CRS) model posits that the excess ^{210}Pb input to the sediments has remained constant over time. In this situation, the rapid accumulation of bulk sediment dilutes the entering excess ^{210}Pb, resulting in low activity in the deposits. Slower bulk sedimentation rates, on the other hand, result in increased ^{210}Pb activity in accumulated sediment [28].

2. MATERIALS AND METHODS

2.1 Experimental Design

Field and laboratory examinations took place bi-monthly for a total of eighteen months, with sampling taking place during both the rainy and dry seasons. Three sampling points in generally undisturbed parts of the river were established at 1000m intervals before the experiment began (Fig.1). In 2011/2012, a Uwitec gravity corer with a 10cm internal diameter was used to collect sediment cores and surface deposits from shallow marginal areas at three locations in the upper Bonny Estuary. In order to get the most accurate date, the sediment was left completely undisturbed during collection. The cores were

then taken to the lab, where they were cut into 2cm slices, dried, and powdered to determine the water and organic matter content. Furthermore, the vertical profiles of ^{226}Ra, ^{210}Pb and its daughter nuclides (^{210}Bi and ^{210}Po, ^{214}Pb, ^{228}Ac, ^{208}Ti amongst orders) activities were determined by alpha and gamma detection. The total hydrocarbon content and total phosphorus down the core were also determined while the temporal and spatial distribution of ^{210}Pb, ^{232}Th and ^{238}U daughters were determined for sub-surface sediment samples collected. The fluxes of ^{210}Pb were used to determine the ages of sediment, sedimentation and accumulation rates while ^{137}Cs was used as chronological markers for the validation of ^{210}Pb dates.

2.2 Field Mapping and Sample Collection

Along the Bonny River, samples were taken at 1000 meter intervals at three different locations. Along the downstream segment of the Bonny River system, Sample Station 1 is located between latitude 4°45'04.03"N and longitude 7°00'14.08"E. The sampling station is located between the Nembe waterside and the Ibeto cement bagging factory's dock area. Sample Stations 2 and 3 are located between latitudes 4°44'12.21"N and 4°46'33.73"N, and longitudes 7°00'01.15"E and 7°00'18.85" respectively along the upstream section of the Bonny River system (Fig.3). The sampled points are at the wharf of the Nigerian Ports Authority (Station 3) and at a point close to the oil terminal (Station 2). Nevertheless, both locations receive refinery effluents, which passes through the dug-in channels from petroleum tank farm to the discharge points into the Bonny River.

In 2011, a Uwitec gravity corer with a 10cm internal diameter was used to retrieve sediment cores from shallow marginal areas at the three locations. Stations 1 (St-1) and 2 (St-2) each had 32 cm and 30 cm cores, respectively, but station 3 (St-3) only had a 20 centimeter core. Furthermore, sediment surface samples (6cm depth) were taken from the three locations throughout various months (August, October, December, February, April, and June) to cover both wet and dry seasons. The cores were immediately sent to the laboratory following retrieval for pre-treatment and conditioning before radiometric analysis. Wet sub-samples were weighed and dried in a continuous temperature drying oven (24 h at 80°C) after each core was sectioned into 2-cm slices. For the three cores, dry samples were weighed again, and the water content in each stratigraphic level was estimated. The water content of each slice was used to calculate bulk densities. Finally, dried sediments were ground to a fine powder in a mortar in preparation for alpha and gamma analysis.

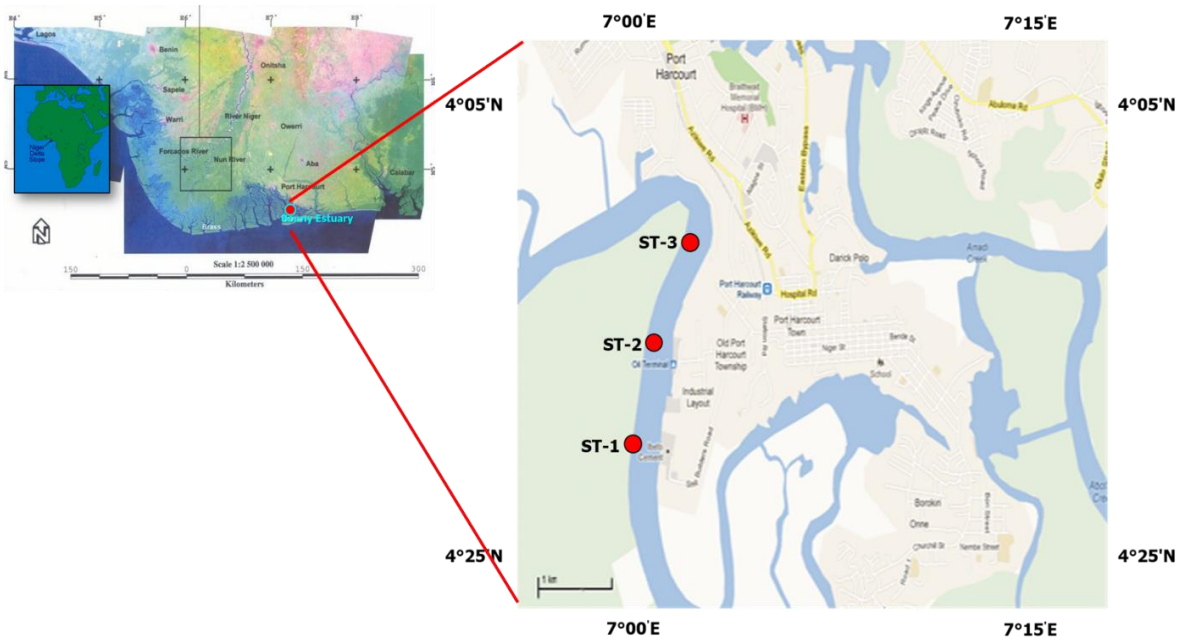

Fig. 3. Enlarged Aerial Map of Bonny Estuary showing Sample Stations

2.3 Radiochemical Analyses of Sediment Cores

2.3.1 Radionuclides by alpha spectrometry

In alpha spectrometry, total ^{210}Pb activity was measured by alpha counting of the daughter radionuclide ^{210}Po. The radiochemical procedure for the determination of ^{210}Po in sediment was based on the isolation of Po from the other elements by self-deposition on silver disc. The deposition was very specific and was carried out in the presence of many other radionuclides in the order of the following procedures:

a. A known amount of dried sample was weighted in a glass beaker and the addition of a weighed aliquot of polonium tracer (^{208}Po or ^{209}Po).
b. Samples were digested using concentrated acids (HNO_3 and HCl).
c. The residue was dissolved in HCl and evaporated to near dryness and further dissolved in about 40 ml of HCl 0.5N
d. The solution was transferred to a 100 ml beaker
e. Subsequently, the original beaker was rinsed with HCl 0.5N and transferred to the solution (making a total volume of 80 ml).
f. A silver disc coated on one side with heat-resistant tape was placed in the bottom of the beaker.
g. The solution was placed on a hot plate at a temperature of about 80°C and stirring was carried out occasionally.
h. After about 6 hours, the disc was removed from the solution and rinsed with H_2O and ethanol and was allowed to dry. The Po source was ready to be counted in an alpha spectrometer.

2.3.2 Radionuclides by gamma spectrometry

The ability to measure emitters directly in the original sample without the requirement for chemical separation is a significant advantage of gamma-ray spectrometry. A CANBERRA high-purity germanium gamma-ray spectrometer was used to examine gamma emitting radionuclides [228Ac (^{228}Ra), ^{214}Bi (^{226}Ra), ^{212}Pb (^{228}Th), and ^{40}K]. For the 1332 keV ^{60}Co-peak, the relative efficiency was 30% and the resolution was 2 keV. Weighed samples were placed in 20 mL nalgene containers and sealed to capture the gaseous ^{222}Rn and ^{220}Rn produced by in-situ ^{226}Ra and ^{224}Ra, respectively. Before counting, the flasks were kept for more than 21 days. Due to the limited amounts of sediment in the upper layers of each core, we had to combine two to three nearby sub-samples in some cases to get the working geometry. At 609.3 keV, ^{226}Ra was produced from the ^{214}Bi photopeak. Because of the low activity of ^{137}Cs and the small amounts of sub-samples (about 20 g), an HPGe detector with a relative efficiency of 70% was utilized to determine this radionuclide at each stratigraphic level. The detector efficiency, gamma intensity, and sample weight were used to determine the specific activity (in Bq.kg-1) in each sample of all the radionuclides investigated. With the help of reference material, the analytical technique was double-checked (IAEA-327). Certified values had good agreement, with > 90% in all cases.

2.4 Determination of Geoaccumulation Index

The geoaccumulation index (*Igeo)* values were calculated for the different metals as described by Muller [29] as follows**:**

$$I_{geo} = \log_2 \left(\frac{Cn}{1.5xBn!} \right) \qquad equ1$$

Where:

Cn= the measured concentration of element 'n' in the sediment
B= the geochemical background for the element 'n'
1.5= is possible variations of the background [30]
However, Muller [29] proposed seven grades or classes of geo-accumulation index**:**

Class 1
Practically uncontaminated

$= I_{geo} < 0$ Class 1

Uncontaminated to moderately contaminated

$=0 < I_{geo} < 1$;

Class 2
Moderately contaminated

$= 0 < I_{geo} < 2$;

Class 3
Moderately to heavily contaminated

$= 2 < I_{geo} < 3$;

Class4
Heavily contaminated

$= 3 < I_{geo} < 4$;

Class 5
Heavily to extremely contaminated

$= 4 < I_{geo} < 5$;

Class 6

Extremely contaminated

$= 5 < I_{geo}$.
Class 6 is an open class and comprises all values of the index higher than class 5. The elemental concentrations in class 6 may be hundred fold greater than the geochemical background value.

2.4 Sedimentation Rate Modelling

2.5.1 Constant initial concentration model (CIC)

The CIC model was applied using the formula below, which assumed a constant ^{210}Pb flux into the sediment and a constant sedimentation rate.

a. $A = Aoe^{\lambda t}$ *equ2*
b. $A = Aoe^{\lambda (x/s)}$ *equ3*
c. $\ln A = -(\lambda/S)x + \ln Ao$ *equ4*

Where

A = activity of excess Pb-210 in the sediment at any depth
Ao= Activity of excess Pb-210 in freshly deposited sediment at depth =0(the sediment-water interface)
S= Sedimentation rate in cm /year
λ= Radioactive decay constant (0.0311/year)
t= Time in year
x = excess used

2.5.2 Constant rate of supply model (CRS)

The CRS which takes care of the nonlinear situation of the sedimentation rate but still assumes constant rate of ^{210}Pb fluxes was applied using the total inventory of the ^{210}Pb excess as in the formula below**:**

$S = Ao/Ax * \lambda x$ *equ5*

Where:

S= Sedimentation rate
Ao= total ^{210}Pb inventory
Ax= activity of excess ^{210}Pb at any depth x
λ = Radioactive decay constant (0.0311/year)

2.6 Statistical Analysis

The data collated were analyzed statistically using statistical analysis software ANOVA to obtain the mean, standard deviation, error range and statistical differences of ($P<0.05$).

3. RESULTS AND DISCUSSION

3.1 Temporal Trends of ^{226}Ra and ^{228}Ra in Surface Sediment

The data obtained for radionuclides are presented in Fig. 4 below, it illustrates the temporal variations of Ra isotopes (^{226}Ra and ^{228}Ra). ^{226}Ra values, which ranged from > 15.67 ± 3.05 to < 34.06 ± 3.61 Bq.kg^{-1} dry weight for all stations during wet and dry seasons while ^{228}Ra were ranged > 33.54 ± 2.64 and < 47.78 ± 2.82 Bq.kg^{-1} dry weight for all station during wet and dry seasons.

The temporal variations of Ra isotopes (^{226}Ra and ^{228}Ra) showed a fairly uniform distribution among locations and months (within error range) with ^{228}Ra, while ^{226}Ra displayed some variability with generally lower specific activities in dry months than in rainy months. The behaviour of these two radioisotopes of radium in estuarine sediment is known to be quite different [31]. Indeed, ^{228}Ra can be more easily desorbed from particles than ^{226}Ra so that the mobility of the former should be lesser than that of ^{228}Ra. Furthermore, ^{226}Ra to ^{228}Ra ratios were also investigated for sediment erosion and accretion as suggested in previous studies [32] and more recently Dai *et al.,* [33]. According to these authors, values lesser than one suggest accretion, and vice versa, and the larger sediment accumulation rates yields to lower ratio of ^{226}Ra/^{228}Ra in surface sediment.

The values found in this study are all less than the unity ranging from 0.3 to 0.8, suggesting accretion and that the three studied sites were sedimentation zones with different sedimentation regimes. The result is in conformity with that of Dublin-Green [34] where a net accretion was reported to be occurring in the upper Bonny Estuary using the distribution pattern of skewness and kurtosis. In addition, the highest values (lowest accumulation) registered during the rainy months attributable to two possible effects: desorption of ^{228}Ra to less contaminated water and, in minor extent, relatively strong water turbulence that reduced the settling of fine particles.

3.2 Temporal Distribution of Total ^{210}Pb in Surface Sediment

Total ^{210}Pb in surface samples collected for more than one year was determined via its daughter ^{210}Po by alpha spectrometry, which assumed that the secular equilibrium between both radionuclides was achieved. Specific activities corrected to the sampling dates are plotted in Fig. 5. The activities in Station 3 (79 Bq.kg^{-1} dw,73 Bq.kg^{-1} dw and 56 Bq.kg^{-1} dw) were found to be lower than those in Station 1(121 Bq.kg^{-1} dw,120 Bq.kg^{-1} dw and 131 Bq.kg^{-1} dw),with Station 2 (92 Bq.kg^{-1} dw , 116 Bq.kg^{-1} dw and 128 Bq.kg^{-1} dw) having the lowest activity (56 Bq.kg^{-1} dw) registered in the sample collected in December (dry month).The unsupported component of ^{210}Pb in estuarine sediment came from two places: the atmosphere, which should be the same for all three stations given their close vicinity, and ^{210}Pb adsorbed onto particles delivered by river inputs and/or dredging activities. As a result, the low ^{210}Pb specific activity in surface sediment could be due to St-3's low sedimentation rate.

3.3 Vertical Distribution of Radionuclides

The specific activities of ^{228}Ac (^{228}Ra), ^{212}Pb (^{228}Th) and ^{40}K against depth in the sampled sediments are plotted in Fig. 6. It was observed that ^{228}Th and ^{228}Ra activities were almost equal to one another at each layer (^{228}Th/^{228}Ra activity ratios ranged from 0.95 ± 0.08 to 1.02 ± 0.08 for St-1, from 0.86 ± 0.17 to 1.02 ± 0.19 for St-2 and from 0.94 ± 10.12 to 1.01 ± 0.16 for St-3 while ^{40}K values ranged from > 210.38 ± 56.78 to < 496.7 ± 33.45 for stations 1, 2 and 3 respectively. In addition, the values obtained for organic matter ranged from 24.6 to 25.8%; 25 to 27.6% and 22 to 8% for stations 1, 2 and 3 respectively.

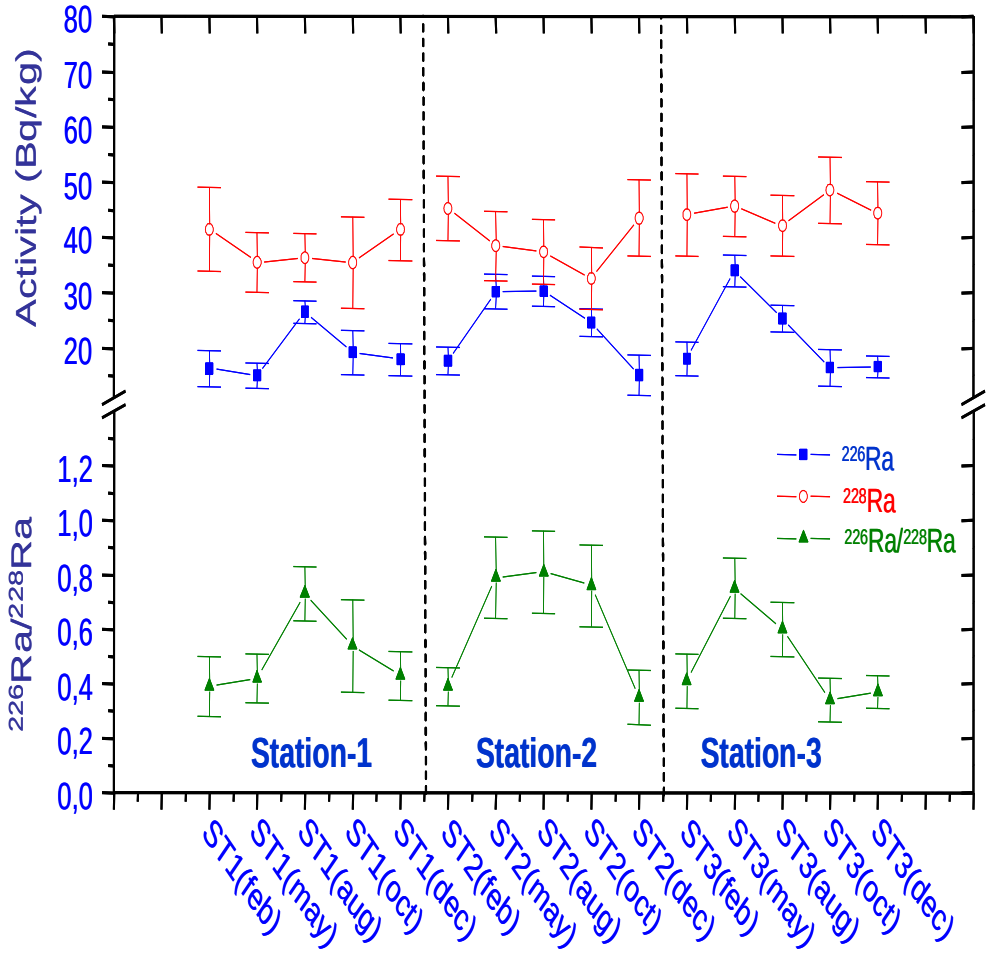

Fig. 4. Temporal Trends of ^{226}Ra and ^{228}Ra in surface sediments. Activities are in Bq.kg^{-1} dry weight and uncertainties are 1-σ statistical errors

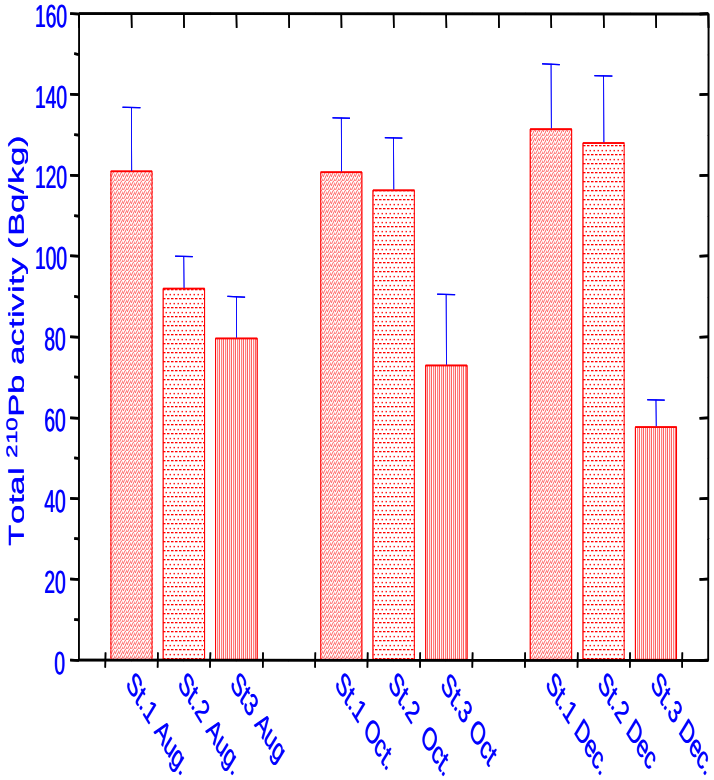

Fig. 5. Temporal distribution of total ^{210}Pb (Bq.kg^{-1}, dry weight) in surface Sediment

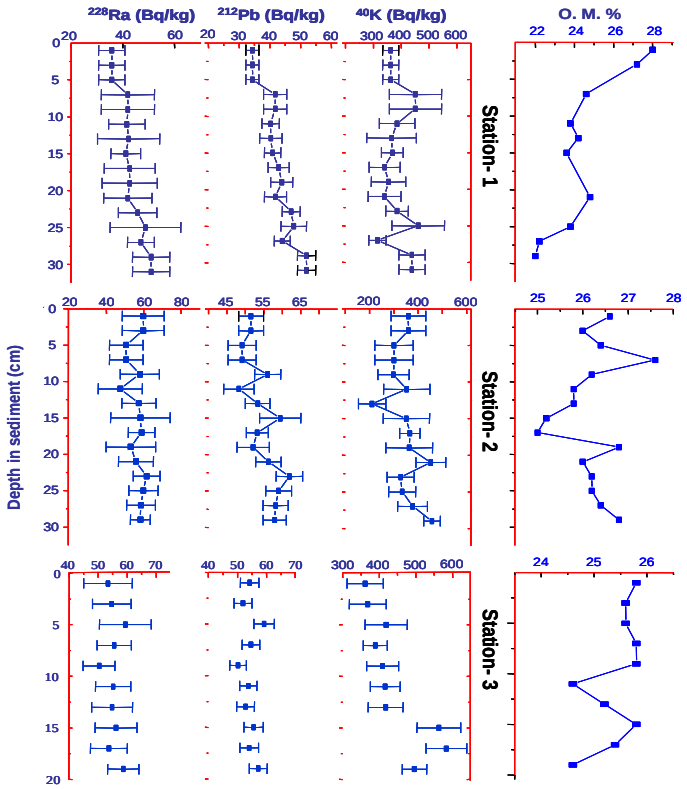

Fig. 6. Vertical distributions of ^{228}Ra, ^{212}Pb and ^{40}K in the three sampled sediment cores

The profiles displayed fairly homogenous distributions throughout the cores with the only exception being ^{40}K in St-3. A relatively visible increase of this radionuclide concentration in the basal 6-cm interval of the core was observed. The enhancement of ^{40}K may be attributed to the differences in the origin of the particles present in the deepest layers of the core that thus may contain more fine-grained clay sediments than the rest of the core. Vertical distributions of organic matter content were also depicted in Fig. 6 for each coring site.

Activities are in $Bq.kg^{-1}$ dry weight and errors are 1-σ statistical uncertainties ^{40}K is a radionuclide, which is indicative of presence of fine-grained clay sediments in harbour and channel environments [35]. The values of ^{40}K found in the core samples collected at different months ranged between 264 and 462 $Bq.kg^{-1}$ dry weight; displaying moderate variability among various months and stations. The values were within the range of values found in coastal environments worldwide [36]. The average specific activities over various months were 388 ± 89 $Bq.kg^{-1}$ for St-2 and St-3, and 326 ± 90 $Bq.kg^{-1}$ for St-1. Therefore, no significant enhanced concentrations were recorded within the error margins of the radionuclide that could identify preferential sites and/or months for deposition of particles.

3.4 Profiles of Radionuclides in the Sediment Cores

The total ^{210}Pb and ^{226}Ra activities in the three cores are presented in Fig. 7 below. The vertical distribution for the Station 1 has values ranging from > 103.1 ± 6.94 to < 172.1 ± 11.26$Bq.kg^{-1}$ dry weight, > 16.70± 3.12 and < 29.69 ± 4.86 $Bq.kg^{-1}$ dry weight for total ^{210}Pb and ^{226}Ra respectively. In Station 2, they ranged from > 70.38 ±3.15 to < 99.74 ± 4.87 $Bq.kg^{-1}$ dry weight for both total ^{210}Pb and ^{226}Ra. The values recorded for the unsupported lead-210 ($^{210}Pb_{xs}$) ranged from > 80.65±8.09 to < 153.64 ± 12.80 and > 45.18±5.32 to < 75.31±6.54 $Bq.kg^{-1}$ dry weight for Stations 1 and 2 respectively.

Furthermore, total ^{210}Pb and ^{226}Ra activities for Station 3 ranged from > 28.59±1.45 to < 93.99 ± 4.58, and >18.92 ± 2.36 to < 44.54 ± 3.06 $Bq.kg^{-1}$ dry weight for total ^{210}Pb and ^{226}Ra respectively. The values for $^{210}Pb_{xs}$ ranged from >10.65 ± 3.28 to < 66.99 ± 4.99 $Bq.kg^{-1}$ dry weight at 0-12cm depth interval.

In addition, the estimated total inventory (the product of activity, bulk density, and thickness of each segment) were 22224, 10480 and 1597± 82 $Bq.m^{-2}$ for Stations 1, 2 and 3 respectively.

The total ^{210}Pb and ^{226}Ra activities throughout the three sediment cores were determined (Fig. 7) with the purpose of carrying out radiometric dating. The vertical distributions corresponding to Stations 1 and 2 showed rather consistent activity with distinct maxima and minima, rather than a dramatic drop in ^{210}Pb with depth. Unsupported lead-210 ($^{210}Pbxs$), which was produced by subtracting the supported fraction (in equilibrium with ^{226}Ra) layer by layer, showed the same variation patterns as total ^{210}Pb and did not drop to zero in the basal layers. As a result, these sediment cores (St-1 and St-2) were classified as incomplete and disturbed and were excluded from $^{210}Pbxs$ sedimentation rates, ages, and total inventories estimates.

Activities with 1-σ statistical errors are all in $Bq.kg^{-1}$ dry weight. On the other hand, ^{226}Ra at Station 3 had an unusual depth distribution, particularly at the 10-12 cm depth interval, and the three basal layers, where the corresponding activities surprisingly exceeded total ^{210}Pb. Such behavior (^{226}Ra > ^{210}Pb) was seen in different environments, but only in the higher core layers [37], which made calculating unsupported ^{210}Pb more challenging. Because ^{226}Ra activity increased as OMC decreased in these layers, this disequilibrium could be partially correlated to the organic matter content (OMC plotted in Fig. 6) in these layers, but the profiles at Stations 1 and 2 did not show any pattern of variation with OMC, making this assumption questionable.

With respect to the profile obtained in the sediment core collected at Station 3, a special assumption was made in an attempt to apply conventional dating models. As total ^{210}Pb activity in the bottom 10-cm depth interval of the sediment core was rather constant, it was assumed that the corresponding activity matched the fraction of supported ^{210}Pb, which was supposed to be constant throughout the core depth [8]. Hence, the excess ^{210}Pb profile presented in Fig. 7 was obtained by subtracting the average activity of the five down-core layers from the measured total ^{210}Pb activity at each depth in the core.

The overall inventory (the sum of the product of activity, bulk density and thickness of each section) was 1597 ± 82 Bq.m^{-2}, which was much lower than the partial inventories for Stations 1 and 2 sediment cores (>22224 Bq.m^{-2} for St-1 and >10480 for St-2). The discrepancies in inventory between sites might be related to horizontal transit within the estuary and, to a large extent, the variability in sedimentation rates at different sites [38]. At Station 3, just a small fraction of the ^{210}Pb derived from the atmosphere was deposited with particles. The yearly flow of ^{210}Pbxs onto sediment at Station 3 was 49.6 2.5 Bq.m-2.y-1, computed as the product of, the ^{210}Pb decay constant, and the total inventory. The unsupported ^{210}Pb has been employed as a chronometer in sediment geochronological research with great success [39].

The CSR (Constant rate of supply) model and CIC (Constant Initial Concentration) model were applied to the $^{210}Pb_{xs}$ profile of the core collected at Station 3. Both models assumed that the input of atmospherically derived ^{210}Pb at a given location is quite uniform over a period of time; or at least close enough to the age of the core. Although $^{210}Pb_{xs}$ activities were different from the values gotten from the least-square fitting when using CIC model, the average sedimentation rate throughout the core obtained from CRS model (0.068 ± 0.015 g.cm^{-2}.y^{-1}) was almost the same to that obtained from CIC model, which was 0.065 ± 0.004. However, the estimated ages were quite different for some layers.

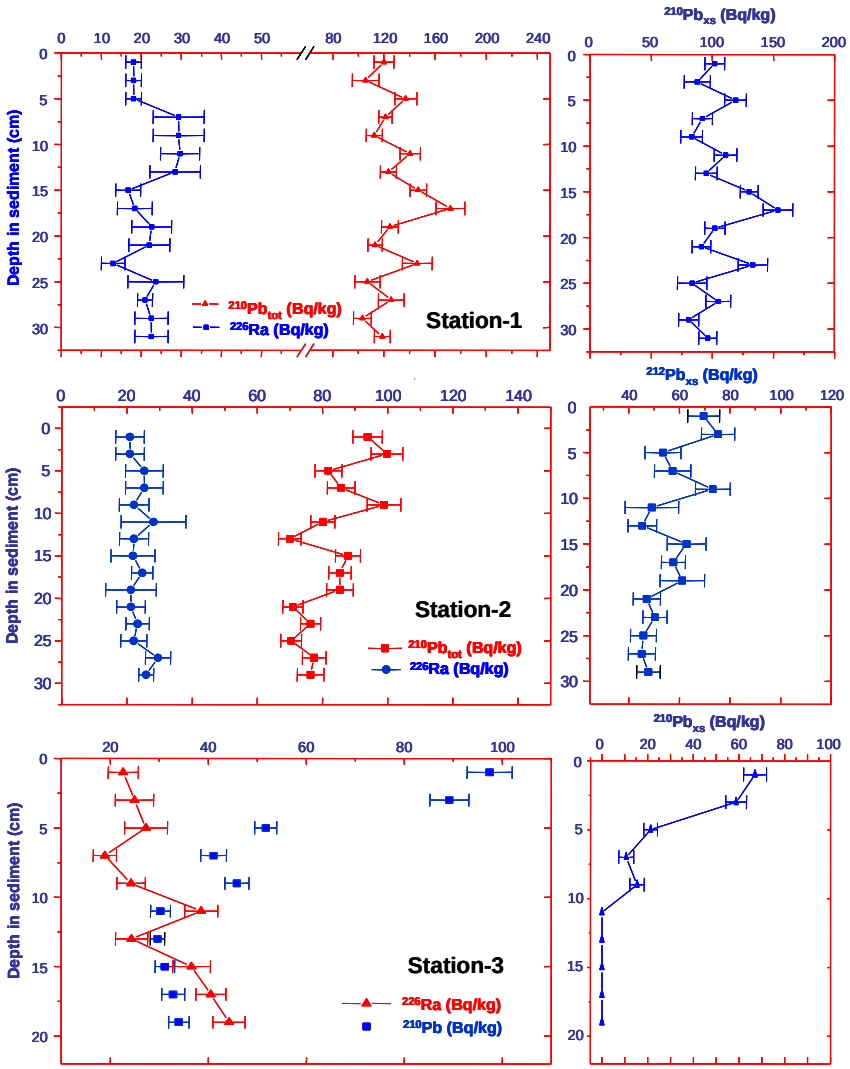

Fig. 7. ^{226}Ra, total ^{210}Pb and $^{210}Pb_{xs}$ activity profiles in the sediment cores collected from the Bonny Estuary

3.5 Ages, Sedimentation Rates and Depth Relationships

The ages and sedimentation rates obtained from the Constant Rate of Supply (CRS) model at each stratigraphic level are displayed in Fig. 8. The values of 0.074 $g.cm^{-2}.y^{-1}$, 0.109$g.cm^{-2}.y^{-1}$, 0.039$g.cm^{-2}.y^{-1}$, 0.550$g.cm^{-2}.y^{-1}$ and 0.064$g.cm^{-2}.y^{-1}$ were obtained as sedimentation rates corresponding with year 2004, 1997, 1973, 1955 and 1943. Although $^{210}Pb_{xs}$ activities are different from the various values provided by the least-square fitting when using Constant Initial Concentration (CIC) model. The average sedimentation rate throughout the core obtained from CRS model (0.068 ± 0.015$g.cm^{-2}.y^{-1}$) was nearly the same as that obtained from the CIC model (0.065 ± 0.004), but the estimated ages were quite different for some stratigraphic layers.

The sedimentation rates calculated suggested low sedimentation which has earlier been reported to signify a very calm environment according to Dublin-Green [34]. It has been reported that the shallow marginal area of the Bonny Estuary is a low energy environment characterized by weak tidal currents (current velocity in the low marginal area is between 20-30cm/sec during flood tide), which promotes the deposition of fine sediments while the deeper channel centres are areas of scourging dominated by strong tidal currents. Values obtained were also in agreement with the observation made during sampling where the flow of the water was seen to be calm and parallel (laminar flow) which is associated with quite environment.

3.6 Validation of ^{210}Pb Ages using ^{137}Cs

^{210}Pb chronology was confirmed by a second independent tracer (^{137}Cs). ^{137}Cs in the sub-samples of the core collected at Station 3. The results are presented in Table 1and values range from below to slightly above the limit of detection by the HPGe gamma spectrometer with 70% relative efficiency.

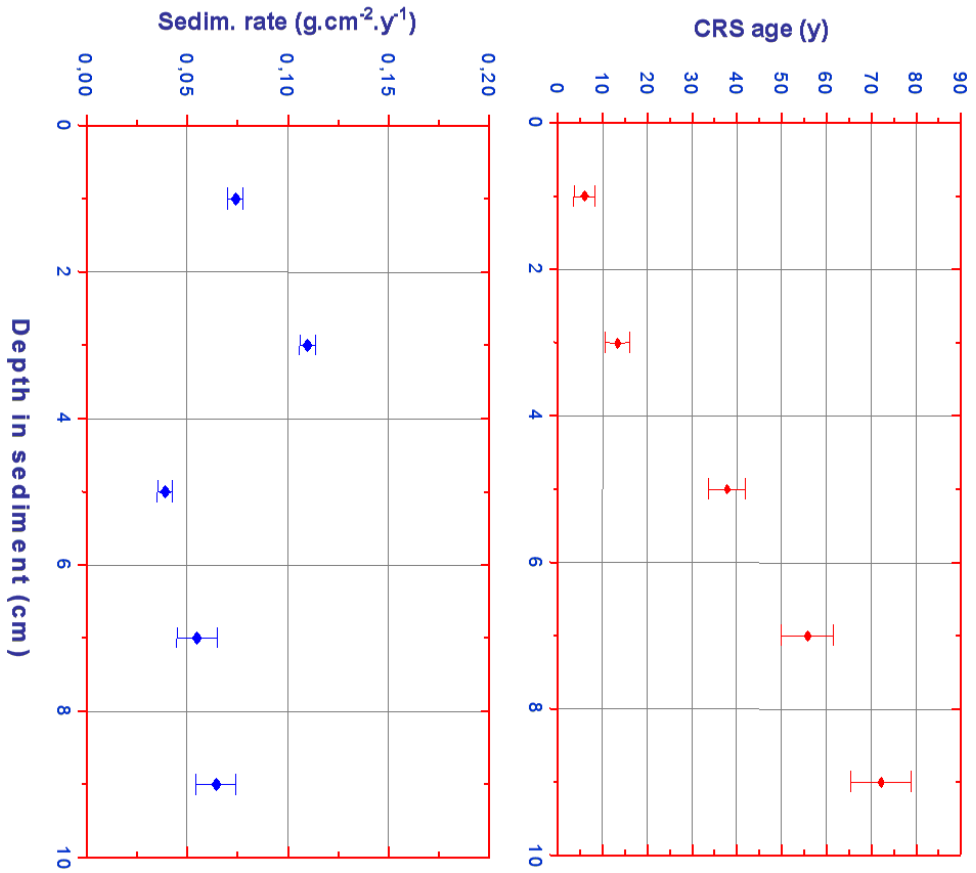

Fig. 8. Age versus Depth; Sedimentation Rate versus Depth relationships determined by CRS Model for the sediment core at Station 3

Table 1. Validation of ^{210}Pb Ages using ^{137}Cs (^{137}Cs activities in Bq.kg^{-1} dry weight in the sampled core collected at Station 3 (LD is limit of detection). Sample depth of 10-20cm was obtained by combining all sub-samples of 2cm thickness

Layer (cm)	Year	^{137}Cs Act. (Bq.kg^{-1})	LD (Bq.kg^{-1})
0−2	2004	<LD	1.496
2−4	1997	<LD	1,521
4−6	1973	<LD	1,825
6−8	1955	1,416 ± 0,112	--
8−10	1938	<LD	1,240
10−20		<LD	0.702

Cesium-137, an artificial radionuclide was the tracer of choice to identify the period of maximum atmospheric fallout resulting from nuclear bomb testing and detonations since early 1950's. The deposition of this radionuclide, however, has been shown to differ in the northern and southern hemispheres based on a comprehensive compilation of its global fallout [40]. It was expected therefore, that ^{137}Cs specific activities (Table 1) in our sediment samples from the Bonny Estuary, being a tropical area, would be relatively low. Effectively, ^{137}Cs in the sub-samples of the core collected at Station 3 as shown in Table 1, were below or slightly above the limit of detection of our detection system (HPGe gamma spectrometer with 70% relative efficiency). Nevertheless, based on the CRS ages, the period of maximum fallout (1963) should be at 6-8-cm depth intervals in the core. The measured activity within this depth interval was 1.416 ± 0,112 Bq.kg^{-1}, and higher than the activity immediately below the 6-8-cm depth intervals (i.e. from 8-10-cm), which was < LD = 1.24 Bq.kg^{-1}.

The activity recorded inside the 6-8-cm depth interval, according to the CRS model, is the mean value of activities of a number of thin layers created over a period of around 15 years. As a result of the modest sedimentation rate, the 2-cm thickness is itself a layered structure (0.124 cm.y^{-1}). As a result, the highest activity from 1963 is diluted in the surrounding silt, which has a low ^{137}Cs concentration. The activities of the upper stratigraphic intervals (0-2cm, 2-4cm, and 4-6cm) were, on the other hand, undetectable due to the small sample size. The detection limits were higher than the particular activity of a depth interval of 6-8cm.

This, combined with the low core resolution (within 2cm depth interval), made determining the depth of the peak associated with the atmospheric weapons testing period extremely challenging. Despite this, individual ^{137}Cs activity detected in the core's basal 10cm depth interval were all less than LD = 1.20 Bq.kg-1, and when combined, they were less than 0.70 Bq.kg-1.

Such discovery assumed that sediment cores below 10cm depth interval in Station 3, where no ^{137}Cs activity was observed (presumably deposited before the onset of the nuclear detonation eras) are in perfect agreement with CRS ages before 1940, according to this research. If there was any ^{137}Cs in these layers, it was due to one or a combination of two factors: first, ^{137}Cs desorption from the overlaying sediment and subsequent diffusion into the deeper stratigraphic intervals; and second, ^{137}Cs desorption from the overlaying sediment and subsequent diffusion into the deeper stratigraphic intervals. Cs has a distribution coefficient that is two to three orders of magnitude lower than highly reactive particles like Pu and Am. [41]. Secondly, ^{137}Cs could cause cross contamination between strata during coring. The occurrence of significant levels of ^{226}Ra, which exceed total ^{210}Pb (Fig. 5), and ^{40}K (Fig. 4) could be due to the large upward movement of Ra-enriched particles with formation water that began in early 1900 during oil exploration and production [42]. Because the potential of these radionuclides to penetrate sedimentary systems is relatively restricted, diffusion of these radionuclides into the sediment column cannot be the cause of their augmentation in deeper stratigraphic layers, as stated by [43].

4. CONCLUSION

The research evaluated the vertical distributions of naturally occurring radionuclides and their temporal trends in sediment cores obtained from three sites in the Bonny Estuary with different sedimentation regimes developed and implemented sediment dating with unsupported lead-210, assessed degree of catchment disturbance in the area by comparing recent sedimentation rates with the pre-European

sedimentation rates. The temporal variations of Ra isotopes showed a fairly uniform distribution among all sampled locations in each month with ^{228}Ra, while ^{226}Ra displayed some variability with generally lower specific activities in dry months than in rainy months. The values found in the study were all less than unity ranging from 0.3 to 0.8, which suggested sediment accretion and that the study area corresponded to zones with different sedimentation regimes. The result is in conformity with that of Dublin-Green [34] where a net accretion was reported to be occurring in the upper Bonny Estuary using the distribution pattern of skewness and kurtosis.

The secular equilibrium between both radionuclides was assumed when the temporal distribution of total ^{210}Pb in surface samples was assessed via its daughter ^{210}Po by alpha spectrometry. Station 3's activities, on the other hand, were found to be lower than those in Station 1, with Station 2 having the lowest activity in the December samples. At each stratigraphic interval, the specific activity of ^{228}Ac (^{228}Ra), ^{212}Pb (^{228}Th), and ^{40}K against depth in the studied cores were found to be nearly comparable. With the exception of ^{40}K in Station 3, the profiles showed rather homogeneous distributions across the cores, which might be attributed to variances in the origin of the particles present in the lowest levels of the sediment core.

The average sedimentation rate throughout the core obtained from Constant Rate of Supply model ($0.068 \pm 0.015 g.cm^{-2}.y^{-1}$) was nearly the same as that obtained from the Constant Initial Concentration model (0.065 ± 0.004). However, the estimated ages were quite variable with depths of various stratigraphic layers. The age of the sediment core was dated approximately 80 years, which was qualitatively validated using ^{137}CS whose activity was definitely undetected in the basal part of the core. The sedimentation rates calculated suggested low sedimentation characterized by low energy environment dominated by weak tidal currents.

COMPETING INTERESTS

Authors have declared that no competing interests exist.

REFERENCES

1. Ajayi TR, N Torto PT. Chokossa; and A. Akinlua. Natural Radioactivity and Trace Metals in Crude Oil: Implication for Health. Environ Geochem Health. 2009;31: 61-6
2. Mokobia CE. Effect of Gamma Irradiation on the Grain yield of Nigerian Zea mays and Arachis hypogaea. J. Radiol. Prot. 2006; 26: 423.
3. Baskaran, M. Radon: A tracer for geological, geophysical and geochemical studies 367. Basel 2016; Springer.
4. Maslennikova A. Holocene environments in the Middle Urals: Palaeolimnological proxies from the Lake Tavatui (Russia). Quat. Int;2022.
5. Heldal HE, Helvik L, Appleby P, Haanes H, Volynkin A, Jensen H, Lepland A. Geochronology of sediment cores from the Vefsnfjord, Norway. Mar. Pollut. Bull. 2021;170:112683.
6. Barsanti M, Garcia-Tenorio R, Schirone A, Rozmaric M, Ruiz-Fernández AC, Sanchez-Cabeza JA, Osvath I. Challenges and limitations of the 210Pb sediment dating method: Results from an IAEA modelling interlaboratory comparison exercise. Quat. Geochronol. 2020;59:101093.
7. Abril JM. Multimodal-TERESA, a ^{210}Pb-based radiometric dating model for recent sediments under largely varying rates of supply. Quat. Geochronol. 2020;55:101032.
8. Cuesta E, Barba-Lobo A, Lozano RL, San Miguel EG, Mosqueda F, Bolívar JP. A comparative study of alternative methods for ^{210}Pb determination in environmental samples. Radiat. Phys. Chem. 2022;191:109840.
9. Tchatchouang Chougong D, Ngueutchoua G, Henock Dicka E, Ekoa Bessa AZ, Youbouni Ghepdeu GF, Bilounga UJF, Armstrong-Altrin JS. Distributions of trace metals and radionuclides contamination in alluvial sediments from the Lobé River in Cameroon. Earth Syst. Environ. 2022;6(1):121-139.
10. Foucher A, Chaboche PA, Sabatier P, Evrard OA. Worldwide meta-analysis (1977–2020) of sediment core dating using fallout radionuclides including ^{137}Cs and ^{210}Pb xs. Earth Syst. Sci. Data. 2021;13(10):4951-4966.
11. George CF, University of Aberdeen, Petroleum Technology Development Fund (Nigeria). Geometries of surface and subsurface landforms and deposits in the Niger Delta;2014.

12. Chima KI, Granjeon D, Couto DD, Leroux E, Gorini C, Rabineau M, Glukstad MM. Tectono-stratigraphic evolution of the offshore western Niger Delta from the Cretaceous to present: Implications of delta dynamics and paleo-topography on gravity-driven deformation. Basin Res. 2022;34(1):25-49.
13. Adeniyi HA, Mbagwu JG. The Assessment of Water Quality of the Jakara Reservoir in Kano State. Ann. Rep. Nat. Inst. Freshwater Fish. Res. Nig. 1983; 89:136-139.
14. Reijers TJA. Stratigraphy and Sedimentology of the Niger Delta. Geologos. 2011;17(3):133-162.
15. NEDECO. The Waters of the Western Niger Delta. Report on an Investigation;1961.
16. Ofomata GEK. Nigeria in Maps: Eastern States. Ethiope Publishing House, Benin City;1975.
17. Pillay KKS, CCJ. Thomas, JA Sandel. Activation Analysis of Airborne Selenium as a Possible Indicator of Atmospheric Sulphur Pollutant. Environ Sci Technol. 1973;5:747
18. Abam TKS. Impact of Dams on the Hydrology of the Niger Delta. Bull. Int. Assoc. Engni Geol. & Environ. 2001; 57: 239-251.
19. Abam TKS, Beets C. Coastal Zone Management Strategy for Hooding and Erosion in the Niger Delta. A Report Prepared for the World Bank;1995.
20. Walling GA, PM. Visscher, AD Wilson, BL Meteir, G Simm, SC Bishop. Mapping of Quantitative Trait Loci for Growth and Carcase Traits in Commercial Sheep Population. J. Anim. Sci. 2004; 82: 22-35.
21. Widdows J, Brinsley MD. Impact of Biotic and Abiotic Processes on Sediment Dynamics and the Consequences to the Structure and Functioning of the Intertidal Zone. J. Sea Res. 2002; 48:143-156.
22. Jie H, Zhinan Z, Zishan Y, Widdows J. Differences in the Benthic pelagic Particle Flux (biodeposition and sediment erosion) at Intertidal Sites with and without Clam (Ruditapes philippinarum) Cultivation in Eastern China. J. Exp.Mar. Biol. Ecol. 2001;261:245-261.
23. Meng X, Kooijman AM, Temme AJ, Cammeraat EL. The current and future role of biota in soil-landscape evolution models. Earth-Sci. Rev. 2022; 103945.
24. Black KS, Tolhurst TJ, Paterson DM, Hagerthey SE. Working with Natural Cohesive Sediments. J. Hydol. Eng. 2002;128: 2-8.
25. Andersen TJ, Jensen KT, Lund-Hansen LC, Mourtisen KN, Pejrup M. Enhanced Erodability of Fine-grained Marine Sediments. Hydrobia ulvae. J. Sea. Res. 2005; 48: 51-58.
26. Goudie A, Middleton NJ. Sahara Dust Stoms: Nature and Consequences. Earth-Sci. Rev. 2001; 56:179.
27. Daramola S, Li H, Omonigbehin O, Faruwa A, Gong Z. Recent retreat and flood dominant areas along the muddy Mahin coastline of Ilaje, Nigeria. Reg. Stud. Mar. Sci. 2022;102272.
28. Brenner M, Schelske CL, Keenan LW. Historical Rates of Sediment Accumulation and Nutrient Burial in Marshes of the Upper St. Johns River Basin, Florida, USA. J.Paleolimnol. 2001;26: 241–257.
29. Muller G. Index of Geo-accumulation in Sediments of the Rhine River. Geo. J. 1969;2(3):108- 118.
30. Turekian KK, Wedepoi KH. Distribution of Element in Some Major Units of the Earth's Crust. Geol. Soc. Am. Bull. 1961;72: 175-192.
31. Elsingep RJ, Moore WS. ^{226}Ra and ^{228}Ra in the Mixing Zones of the Pee Dee River-Winyah Bay, Yangtze River and Delaware Bay Estuaries. Estuar. Coast. Shelf Sci. 1984;18:601-613.
32. Bai ZG, Wan GJ, Wang CS. Geochemical Speciation of Soil ^{7}Be, ^{137}Cs, ^{226}Ra, ^{228}Ra as Tracers to Particle Transport. Pedosphere. 1997;7(3):263–268.
33. Dai A. Characteristics and trends in various forms of the Palmer Drought Severity Index during 1900. 2008. J. Geophys. Res. Atmos. 2011;116(D12).
34. Dublin-Green CO. Some Textural Characteristics and Organic Matter Contents of Recent Sediments in the Bonny Estuary, Niger Delta. Technical Paper. 1985;N°67.ISBN:978-2345-069.
35. Noakes S. Post Disposal Areal Mapping of Sediment Chemistry at the Fort Pierce, Florida ODMDS. U.S. Environmental Protection Agency, Final Report; 2003.
36. UNSCEAR. Sources, Effects and Risks of Ionizing Radiation. Report to the General Assembly (New York: United Nations). 2000; 65

37. Brenner M, Peplow AJ, Schelske CL. Disequilibrium between ^{226}Ra and supported ^{210}Pb in a sediment core from a shallow Florida lake. Limnol. Oceanogr. 1994; 39(5):1222-1227.
38. Heltz GR, Setlock GH, Cantillo AY, Moore WS. Processes Controlling the Regional Distribution of ^{210}Pb, ^{226}Ra and Anthropogenic Zinc in Estuarine Sediments. Earth & Planet. Sci. Let. 1985; 76: 23-34.
39. Laissaoui A, Benmansour M, Ziad N, IbnMajah M, Abril JM, Mulsow S. Anthropogenic Radionuclides in the Water Column and a Sediment Core from the Alboran Sea. Application to Radiometric Dating and Reconstruction of Historical Water Column Radionuclide Concentration. J. Paleolimnol. 2008; 40(3), 823-833.
40. Pfitzner J, Brunskill G, Zagorskis I. ^{137}Cs and excess ^{210}Pb Deposition Patterns in Estuarine and Marine Sediment in the Central Region of the Great Barrier Reef Lagoon, North-eastern Australia. J. Environ. Radioact. 2004;76:81–102.
41. International Atomic Energy Agency. Sediment Distribution Coefficients and Concentration Factors for Biota in the Marine Environment. Technical Reports Series. 2004; ISSN 0074–1914; 422.
42. Kolb WA, Wojcik M. Enhanced Radioactivity Due to Natural Oil and Gas Production and Related Radiological Problems. Sci. Total Environ. 1985; 45: 77–84.
43. Ligero RA, Feria F, Casas-Ruiz M, Corredor C. Diffusion of ^{226}Ra and ^{40}K Radionuclides Reproduced in Underwater Sedimentary Columns in Laboratory. J. Environ. Radioact. 2006;87:325-334.

Peer-review history:
The peer review history for this paper can be accessed here:
https://www.sdiarticle5.com/review-history/85282